Impact of bubbles on the light field within a photobioreactor: a practical design tool Supplementary materials

Victor Pozzobon[1] ✉

[1]LGPM, CentraleSupélec, Université Paris-Saclay, Centre Européen de Biotechnologie et de Bioéconomie (CEBB), 3 rue des Rouges Terres 51110 Pomacle, France

Convergence - Fluid dynamics

Figure 1 presents the average sliding velocity of the bubble swarm in the two extreme cases (lowest and highest void fraction). As one can see, the simulations can be considered converged after 15 seconds. Afterwards, the fluctuations are minimal, and no trend can be detected. Consequently, the simulations were run for four times the convergence time.

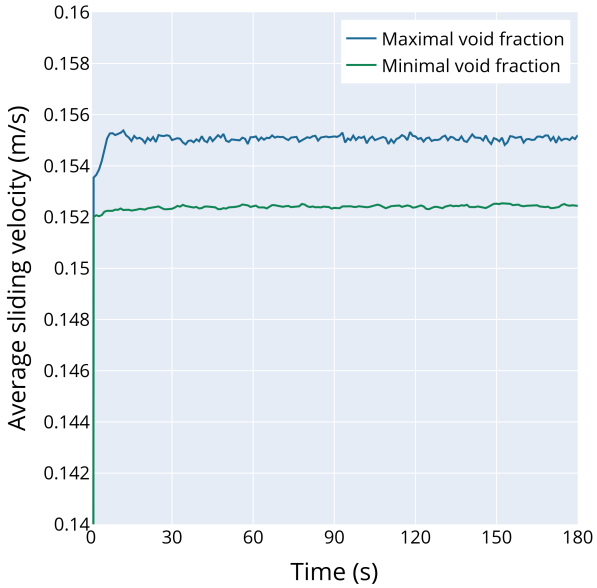

Fig. 1. Average sliding velocity over time, at minimal and maximal average void fractions

Once a time long enough to ensure convergence has been identified, the next step was to ensure the absence of artifacts and that the domain size was large enough to prevent spatial correlation between the inlet and the outlet. Regarding the first indicator, Figure 2 shows the bubble swarm distribution in space along the three axes. No significant concentration of bubbles can be detected, which is a token of the quality of the results.

Then, Figures 3 and 4 present nephogram plots of the local void fraction within the domain, with a spatial resolution of four bubble diameters, at 59 and 60 seconds, respectively. As one can see, no spatial or temporal correlation can be drawn between the two frames. This indicates that the domain is large enough to produce a representative fluid dynamic scene,

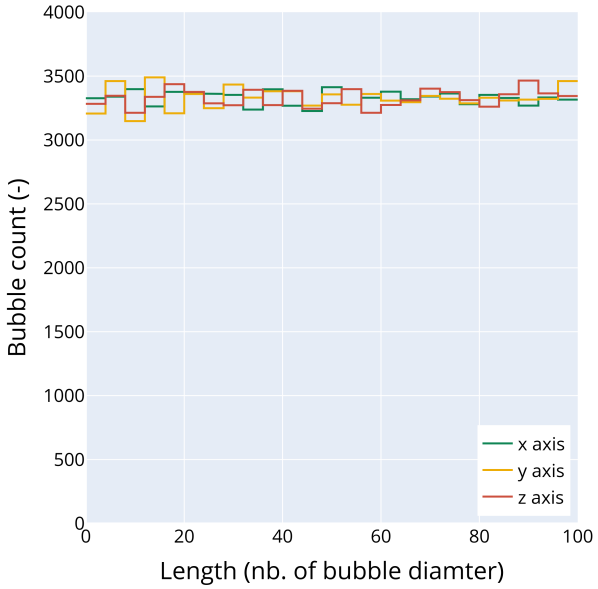

Fig. 2. Bubble distribution along the x, y, and z axis, at maximal average void fraction, step size of four bubble diameters, time: 60 s

and the scene can be sampled at one-second intervals if multiple bubble positions distributions were needed.

Convergence - Ray Tracing

As the optical scene features non-physical lateral boundaries, it was mandatory to lead the calculations in a domain larger than the one that was actually going to be studied. In this case, a domain size of 100 bubble diameter was chosen. To determine the size of the core (unaffected by the lateral boundaries) of the domain, regions of consecutively wider size were extracted and compared. Figure 5 presents the pairwise comparison of all the possible extractions (1 bubble diameter size increment). As one can see, too-small inner domains (from 2 to around 15 diameters) are not comparable. Then, the similarity starts to appear (from around 15 to about 20 diameters). Then, a valid zone can be distinguished (from about 20 to around 80 diameters). Finally, a zone where similarity decreases (because of the lateral boundaries appear). Consequently, a subdomain size of 50 diameters was chosen.

Then, independence to the number of rays was investigated. Figure 6 reports the light absorption profile within the domain (subsample of 50 bubble diameters) for different numbers of rays cast into the scene. As one can see, the over-

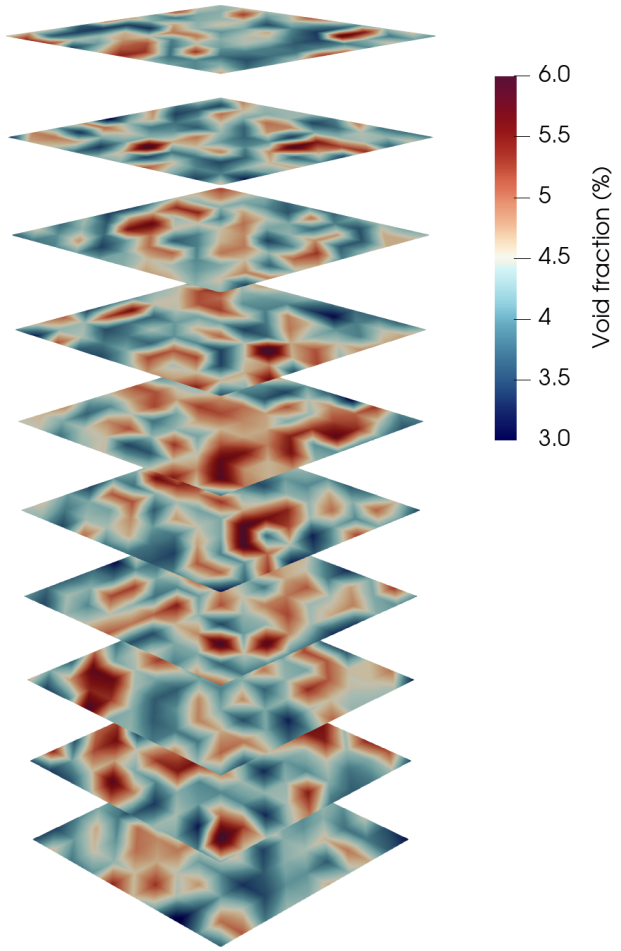

Fig. 3. Nephogram of the local void fraction, at maximal average void fraction, time: 59 s

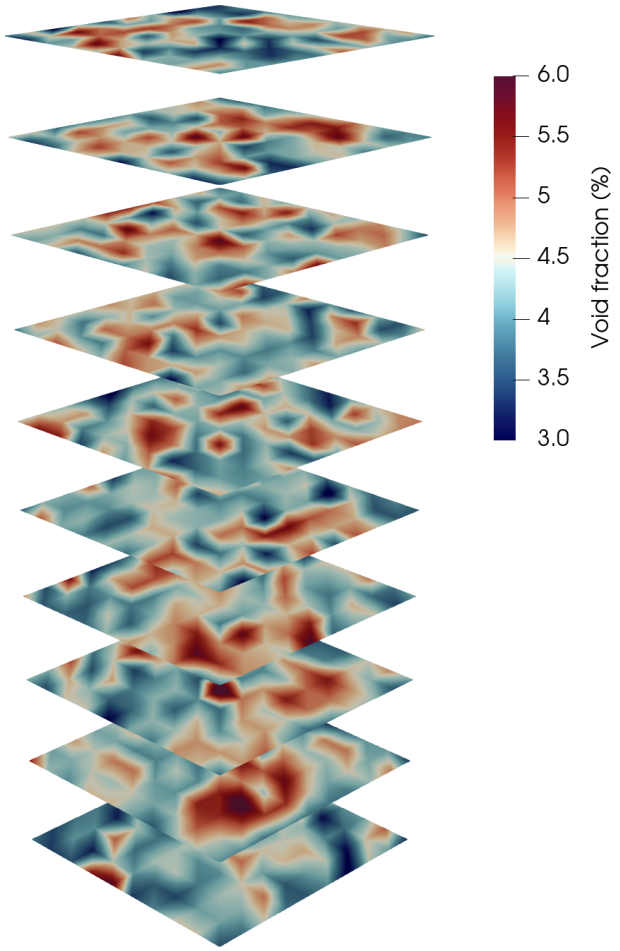

Fig. 4. Nephogram of the local void fraction, at maximal average void fraction, time: 60 s

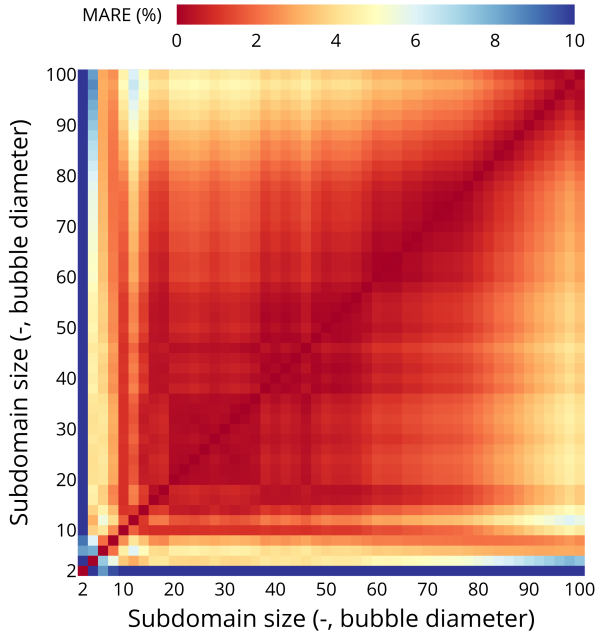

Fig. 5. Subdomain size comparison using Mean Absolute Relative Error (MARE) of all the possible pairwise combinations. Number of ray for the whole scene: 100 billion. π_3 = 0.54 %, π_4 = 0.05, π_5' = 0

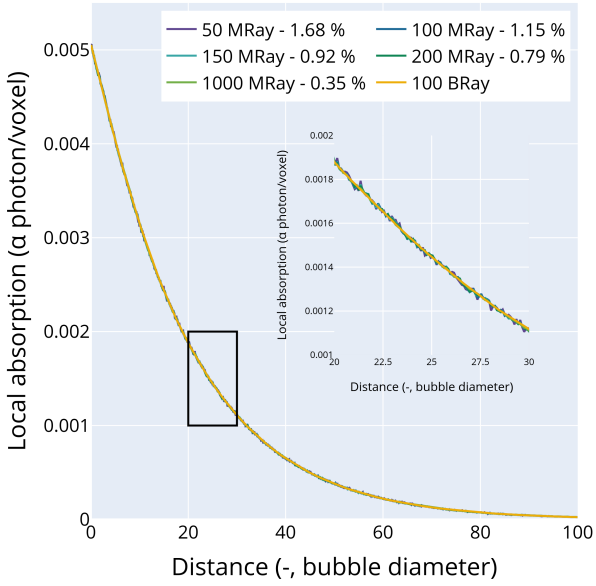

Fig. 6. Local light absorption profile within the domain (subsample of 50 bubble diameters) for different number of rays cast into the scene. Percentage next to the number of rays: MARE. π_3 = 0.54 %, π_4 = 0.05, π_5' = 0

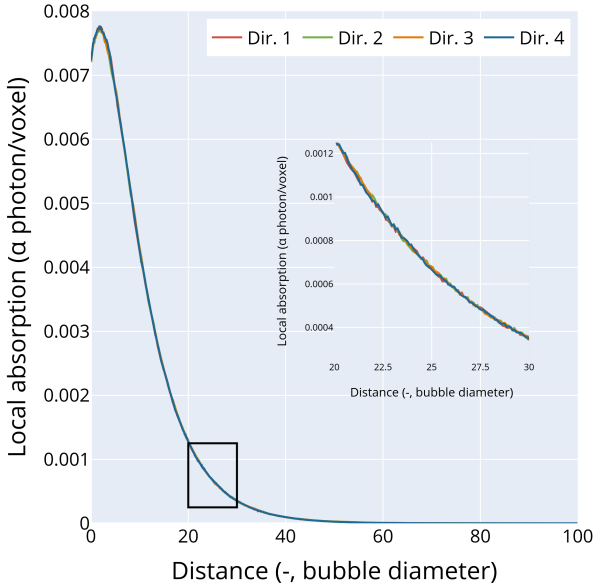

Fig. 7. Local light absorption profile within the domain (subsample of 50 bubble diameters, 150 million rays) for different orientations of the scene

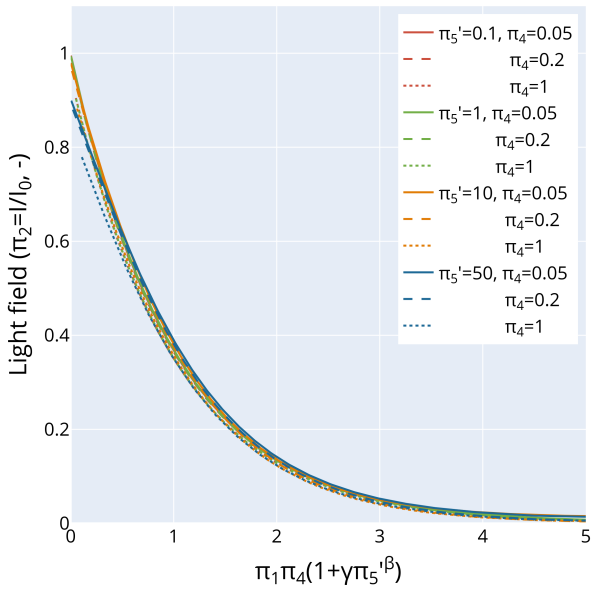

Fig. 8. Light field within the domain without bubbles. Scaled dimensionless abscissa (with γ = 0.02479 and β = 0.9848)

all trend is captured with only a few rays. Yet, as the number of rays increases, the profiles become increasingly smoother. A criterion had, therefore, to be chosen. In this case, it was decided that a deviation (evaluated with the Mean Absolute Relative Error) of 1 % percent from the reference simulation (100 B rays) was acceptable. This criterion yielded a number of 150 million rays to be cast.

Both tests were led with the configuration deemed the most stringent, *i.e.*, the lowest void fraction (0.54 %), the lowest cell light absorption (π_4 = 0.05), and no cell scattering (π_5' = 0). Indeed, in this case, the rays are prone to escape the scene, and therefore, the lowest amount of information is gathered, making this configuration extremely demanding.

One final test was to be carried out to determine the number of scenes to be used to ensure domain convergence. Indeed, as the scenes are generated using fluid dynamics, scene-to-scene variation may exist. Several actions can be taken to alleviate this problem (in order of efficacy and computational power greediness): generate more fluid dynamics simulation (with random bubble position initialization), extract different scenes from a simulation (provided they are sufficiently distant from each other), or rotating a scene to light the four lateral faces successively. In order to evaluate the need for one or more of these approaches, the scene rotation was first evaluated. The setup chosen was the one inducing the largest amount of ray interaction within the scene, *i.e.*, highest void fraction (4.30 %), lowest absorption (π_4 = 0.05), and highest cell scattering (π_5' = 50). Figure 7 presents the results for the four orientations of the scene. As one can see, the local absorption profiles are markedly similar. In addition to qualitative observation, the difference can be quantified. Here again, the MARE was used. The scenes were compared in a pairwise manner (so long the point on the profile represents at least 1 % of the maximum value to avoid artificial overestimation in the low-signal region, *i.e.*, a long tailing effect).

Overall, the average discrepancy between the scenes is 1.06 ± 0.19 %. Given the low value obtained is the most dire configuration, it was concluded that only one scene could be evaluated per case.

Illumination profile scaling

Figure 8 presents the selected illumination profiles scaled with the expression of the shape $\pi_1\pi_4(1+\gamma\pi_5'^{\beta})$ (values: 0.02479 and 0.9848 for γ and β, respectively).

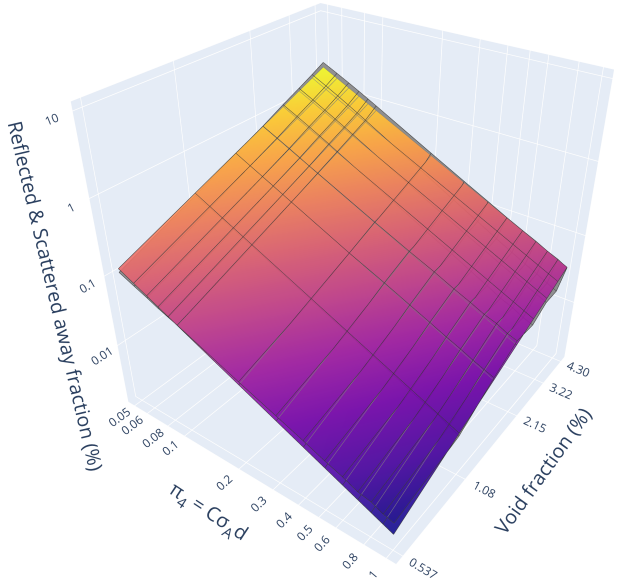

Fig. 9. Reflected and scattered light response surface as a function of void fraction and optical thickness. Gray surface - simulations. Colored surface - proposed model. Microalgae scattering was nullified, i.e., π_5' = 0. Surface color is equivalent to z axis

Bubble scattering contribution

A multilinear regression was led in logarithmic space to minimize the RMSD on the reflected and scattered light fraction in the $\pi_4 \times \alpha$ space. The first process was led by letting the single parameter contributions free, which yielded Equation 1. As one can see, the coefficients of the variables are quite similar and close to 4/3. Hence, this value was substituted before running the process again. In terms of RMSD, the value increased by 6.91 %, which was deemed acceptable to remove two parameters from the optimization procedure. In addition, the loss of performance mainly affected the part of the space where the reflected and scattered light fraction was low. Consequently, the influence in the scope of microalgae cultivation can be deemed negligible. Finally, Figure 9 presents the simulation-generated and multilinear regression-approximated data, which are in close agreement.

$$ln(\rho_b) = 1.267\, ln(\alpha) - 1.359\, ln(\pi_4) - 4.014 \qquad \textbf{(1)}$$